

Numerical Study of Separation Length of Flow through Rectangular Channel with Baffle Plates

M. M. Jamil¹, M. I. Adamu¹, T. R. Ibrahim² and G. A. Hashim^{*3}

¹Kano state Ministry for Higher Education, Nigeria.

²Ministry of Electricity, Iraqi.

³Faculty of Mechanical Engineering, Universiti Teknologi Malaysia, Malaysia

*.cghasaq_88@yahoo.com

Abstract – In this paper, Reynolds average Navier stokes models simulation was computed with standard $k-\epsilon$, realizable $k-\epsilon$ and SST $k-\omega$. The three models were proposed to forecast the turbulence flow behaviour inside a rectangular channel with two baffle plates. The geometry and the grid were generated using commercial CFD software fluent. The flow behaviours of three models were characterized based on positions of the entrance to the first baffle, positions between first and second baffle and lastly the second baffle. At the three different positions the three models studied have demonstrate differences in the velocity profiles and separation range. Comparison with previous literatures shows applicability of these three models to produce velocity profile characteristics and separation behaviours. Even though some of the models have shown slight deviation from the experimental results but in general the three models were considered to be in close agreement with most published literatures. Copyright © 2015 Penerbit Akademia Baru - All rights reserved.

Keywords: Baffle plate, Standard $k-\epsilon$, Realizable $k-\epsilon$ and SST $k-\omega$, Rectangular channel and separation

1.0 INTRODUCTION

There are many industrial applications for Flow through channels with baffle plates like heat exchangers, chemical reactors, nuclear industry, filtration and desalination. In shell and tube heat exchangers, the baffle plates are commonly used in the shell-side fluid for flow across the shell. These baffles increase the turbulence and the heat exchange time between the cross flow and hot surfaces. The turbulent flow and heat transfer through a channel with baffle plates has been studied in many experimental and numerical researches.

The cross flow in the banks can be analyse by means of baffle plates for shell-and-tube heat exchangers, which considerably change the direction of the flow and raise the heat exchange time between heated surfaces and fluid . Baffles are used in increasing turbulence levels and heat exchange ratios.

On the other side, boundary layer separation may be observed after the baffles, as demonstrated in some literatures [1]. This can be an additional and important source of disturbances in the flow, which can travel through the bank, influencing the tube bank and the baffles. Möller et al. [2] experimentally reported velocity and wall pressure fluctuations in

the turbulent flow through a simulated tube bank with square baffle plate arrangement. Kelkar and Patankar [3] have studied numerical analysis of laminar flow with heat transfer between parallel plates with baffles, the results show that the flow is characterized by big recirculation regions and strong deformations. Nusselt number and friction coefficient increased with the Reynolds number. Cheng and Huang [4] have analyzed laminar forced convection flows in the entrance region of a horizontal channel. Computations for the semi-infinite channel within which one or two pairs of baffles are symmetrically attached to the respective walls in the entrance region have been performed. Berner et al. [5] studied the forced convection in a channel with baffle plates. They concluded that the laminar behaviour is expected at a Reynolds number below 600. They mentioned that the situation of the flow was free from vortex shedding. Cheng and Huang [4] investigated the case where the transverse baffles are not symmetrically placed. Their results have indicated that the relative position of the baffle arrays is an influential factor on the flow field, especially for baffles with a large height. Habib et al. [6] reported turbulent flow and heat transfer through a duct with baffle plates; he concluded that the heat flux was uniform on the upper and lower walls. The results show that the local and average Nusselt numbers increased with the increase of Reynolds number. Also, the pressure drop increased as baffle height increases. Demartini et al. [7] used experimental techniques to investigate the pressure drop and stream wise velocity distribution of the turbulent flow with baffles in a channel. Guo and Anand [8] have examined three dimensional heat transfers in a channel with a single baffle in the entrance region. De Zilwa et al. [9] studied laminar and turbulent flows through plane sudden-expansions. Turbulent flow simulations were compared to experimental results using $k-\epsilon$ models, results found showed $k-\epsilon$ models to be very reliable, except in recirculation regions near the walls. Antoniou and Bergeles [10] reported flow over prisms using hot wire technique with several aspect ratios. Increased in aspect ratio L/H implies reattachment in the prism surface and downstream, while recirculation lengths and turbulence scales are reduced. Prithiviraj and Andrews [11] studied three dimensional flows in shell and tube heat exchanger. The study was based on fully implicit control calculation procedure. They focused on the spacing between the baffles and pressure drop. Bazdid-Tehrani and Naderi-Abadi [12] conducted a numerical study of the fluid flow and heat transfer in a duct with in line baffles and reported that the heat transfer behaviour of this type of baffles is somehow inefficient for large values of the blockage ratio. However, as noted by earlier articles, for the case of staggered baffles, the converse is true. Generally, bulk temperature values along the duct are decreased with the increase of Reynolds number for most of the cases studied. RachidSaim et al. [13] found that vortex shedding generated by the baffle on the upper wall can additionally enhance heat transfer along the baffle surfaces. M.A. Louhibi et al. [14] concluded that baffles angle inclination has a major effect on isotherms, streamlines and total heat transfer inside the channel. The effect of increase in inclination of the baffle enhanced heat transfer inside the channel and heat transfer becomes very important with addition of baffles.

In this work, the turbulent flow through a duct with rectangular baffle plates is studied. The turbulence was modelled using standard $k-\epsilon$, realizable $k-\epsilon$ and SST $k-\omega$ turbulence model. The aim of the present work is to study the turbulent flow in a duct with three different models of Reynolds Average Navier Stoke models RANS i.e. standard $k-\epsilon$, realizable $k-\epsilon$ and SST $k-\omega$ and compare the separation ability between the three models.

2.0 MATHEMATICAL DESCRIPTION

2.1 Statement of problem

The geometry adopted in this study is a rectangular section channel with two baffles spaced 0.142m in length which is treated as 2D flow without considering heat transfer in the baffle plates. Turbulent flow with Reynolds number 8.7×10^4 was used from experimental result obtained with initial velocity (reference velocity) of 7.8 m/s. The flow is considered to be steady with channel hydraulic diameter of 0.167m defined from Reynolds number relation given below:

$$Re = \frac{\rho D_H U_o}{\mu} \quad (1)$$

Where U_o is the reference velocity, ρ is density, D_H Is the hydraulic diameter. All dimensions in metre (m).

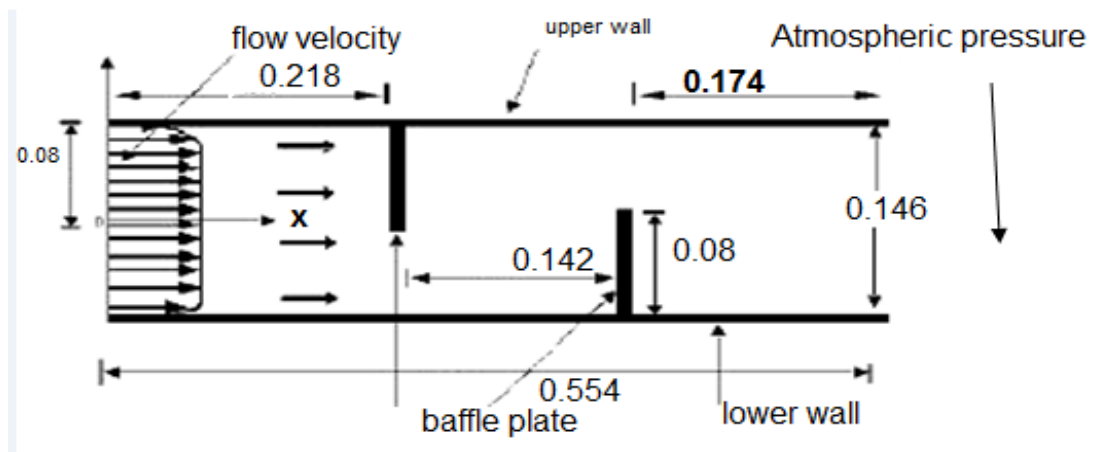


Figure 1: Geometry of a rectangular Cross section with two baffle plates and boundary conditions.

2.2 Governing equations

The governing equations of the turbulence model studied are based on the Reynolds average Navier-stokes equations. More importantly continuity and momentum balance equations are considered in this problem. The Newtonian fluid flow for the two dimensional incompressible flow is given as follows:

$$\frac{\partial U_j}{\partial x_j} = 0 \quad (2)$$

$$\rho \overline{U_j} \frac{\partial \overline{U_j}}{\partial x_j} = \frac{\partial \overline{p}}{\partial x_i} + \frac{\partial}{\partial x_j} \left(\mu \frac{\partial \overline{U_i}}{\partial x_j} - \rho \overline{U_i U_j} \right) \quad (3)$$

Where ρ and p are the constant density and pressure respectively, while \overline{U}_i and \overline{U}_j are mean velocity components in X_i and X_j directions, μ is the dynamic viscosity.

Reynolds stress is given by additional term $\rho \overline{U_i U_j}$.

The Boussinesq hypothesis proposed by Kolmogorov is given by the formulae as follows:

$$-\rho \overline{U_i U_j} = \mu_t \left(\frac{\partial \overline{U}_i}{\partial X_j} + \frac{\partial \overline{U}_j}{\partial X_i} \right) - \frac{2}{3} \rho \delta_{ij} k \quad (4)$$

Where μ_t is the eddy viscosity, δ_{ij} the Kroenecker Delta and k the kinetic energy of the turbulence given by:

$$k = \frac{1}{2} \overline{U_i U_i} \quad (5)$$

The best turbulence models are those that solve two differential transport equations that are based on eddy viscosity addition.

2.3 Boundary conditions

The boundary conditions of the geometry at the inlet region, boundary walls and the outlet region are described as follows. For Inlet region:

$$k = 0.005 U_0^2 \quad (6)$$

$$\varepsilon = 0.1 k_0^2 \quad (7)$$

where k and ε are the kinetic energy conditions for inlet turbulent and inlet dissipation respectively.

For walls:

$$\frac{\partial k}{\partial n} = 0 \quad (8)$$

At the walls both k and ε are equals to zero

For outlet region:

$$\frac{\partial u}{\partial x} = \frac{\partial v}{\partial x} = \frac{\partial k}{\partial x} = \frac{\partial \varepsilon}{\partial x} = 0 \quad (9)$$

The pressure considered at the outside the region is atmospheric with air as working fluid [15].

2.4 Turbulence Model

The standard $k-\varepsilon$ is the most common and popular model used proposed by Launder and Spalding but in this study standard $k-\omega$ was also used proposed by Wilcox. This model

described two transport equations for the k-ε which include the turbulent kinetic energy and the turbulent kinetic dissipation energy. In this case Reynolds average Navier-stokes equations are the governing equations used based on continuity and momentum balance equations. For k-ω model equations the turbulence kinetic energy, dissipation rate and closure coefficient are described below:

Standard k-ε model equations.

$$\rho \frac{\partial k}{\partial t} + \frac{\partial \rho k U_j}{\partial x_j} = \frac{\partial}{\partial x_j} \left[\left(\mu + \frac{\mu_t}{\sigma_k} \right) \frac{\partial k}{\partial x_j} \right] + \rho (Q_k - \varepsilon) \quad (10)$$

$$\rho \frac{\partial \varepsilon}{\partial t} + \frac{\partial \rho \varepsilon U_j}{\partial x_j} = \frac{\partial}{\partial x_j} \left[\left(\mu + \frac{\mu_t}{\sigma_\varepsilon} \right) \frac{\partial \varepsilon}{\partial x_j} \right] + \rho \frac{\varepsilon}{k} (c_{1\varepsilon} Q_k - c_{2\varepsilon} \varepsilon) \quad (11)$$

And the eddy viscosity is defined as:

$$\mu_t = c_\mu \frac{k^2}{\varepsilon} \quad (12)$$

$$Q_k = -\rho \overline{U_i U_j} \frac{\partial \overline{U_j}}{\partial x_i} \quad (13)$$

Equation (13) is based on Boussinesq's hypothesis modeled, where Q_k is also given as:

$$Q_k = \mu_t S^2 \quad (14)$$

where S is the modulus of the mean strain tensor, given by

$$S = \sqrt{2 S_{ij} S_{ij}} \quad (15)$$

And the strain tensor which is symmetrical part of the velocity gradient is given as:

$$S_{ij} = \frac{1}{2} \left(\frac{\partial \overline{U_i}}{\partial x_j} + \frac{\partial \overline{U_j}}{\partial x_i} \right) \quad (16)$$

$$U^* = \frac{1}{\kappa} \ln E y^* \quad (17)$$

where y^* represent the dimensionless distance of the walls.

$$y^* = \frac{\rho C_\mu K_p^{1/2} y_p}{\mu} \quad (18)$$

where κ and E are von Karman constant (0.42) and Empirical constant (9.81m/s) respectively, \overline{U}_p is the time average velocity at position P, K_p is kinetic energy of turbulence at position P and y_p is the distance from position P to the wall.

The constants coefficients of the model are given in the table below:

Table 1: Constant coefficients of the model.

$C_{1\epsilon}$	1.44
$C_{2\epsilon}$	1.92
C_μ	0.09
σ_k	1.0
σ_ϵ	1.3

Transport Equations

$$\frac{\partial}{\partial t}(k) + \frac{\partial}{\partial x_j}(ku_j) = \frac{\partial}{\partial x_j} \left[\left(\mu + \frac{\mu_t}{\sigma_k} \right) \frac{\partial k}{\partial x_j} \right] + P_k + P_b - \rho \epsilon - Y_M + S_K \quad (19)$$

$$\frac{\partial}{\partial t}(\epsilon) + \frac{\partial}{\partial x_j}(\epsilon u_j) = \frac{\partial}{\partial x_j} \left[\left(\mu + \frac{\mu_t}{\sigma_\epsilon} \right) \frac{\partial \epsilon}{\partial x_j} \right] + C_1 S_\epsilon - C_2 \frac{\epsilon^2}{k + \sqrt{\nu \epsilon}} + C_{1\epsilon} \frac{\epsilon}{k} C_{3\epsilon} P_b + S_\epsilon \quad (20)$$

$$C_1 = \max \left[0.43 \frac{n}{n+5} \right], \quad n = S \frac{k}{\epsilon}, \quad S = \sqrt{2S_{ij}} \mu_t = \rho C_\mu \frac{k^2}{\epsilon}$$

where P_k = turbulence kinetic energy due to the mean velocity gradients P_b is the generation of turbulence kinetic energy due to buoyancy.

The eddy viscosity term of k- ω model is defined as:

$$v_T = \alpha^* K / \omega \quad (21)$$

$$u \frac{\partial k}{\partial x} + v \frac{\partial k}{\partial y} = v_T \left(\frac{\partial u}{\partial y} \right)^2 - \beta^* \omega k + \frac{\partial}{\partial y} \left[(\nu + \sigma^* v_T) \frac{\partial k}{\partial y} \right] \quad (22)$$

$$u \frac{\partial \omega}{\partial x} + v \frac{\partial \omega}{\partial y} = \alpha \frac{\omega}{k} v_T \left(\frac{\partial u}{\partial y} \right)^2 - \beta \omega^2 + \frac{\partial}{\partial y} \left[(\nu + \sigma v_T) \frac{\partial \omega}{\partial y} \right] \quad (23)$$

From equation (10) k-turbulence kinetic energy; ω is the specific dissipation rate and σ^* is the closure coefficient. Equation (11) and (12) described the incompressible boundary layers [16].

3.0 NUMERICAL APPROACH

Numerical simulation approach was used with three different methods of Reynolds Average Navier Stokes (RANS) turbulence models which include the Standard $k-\epsilon$, Realizable $k-\epsilon$ and SST $k-\omega$. Commercial CFD software (fluent) was used for the computational meshing using the package existing tools. Standard $k-\epsilon$, Realizable $k-\epsilon$ and SST $k-\omega$ were computed to analyse the flow separation characteristics of the flow with two baffle obstacles. Mesh of the geometry was generated by fluent software (Ansys 14.0) using 20,000 elements.

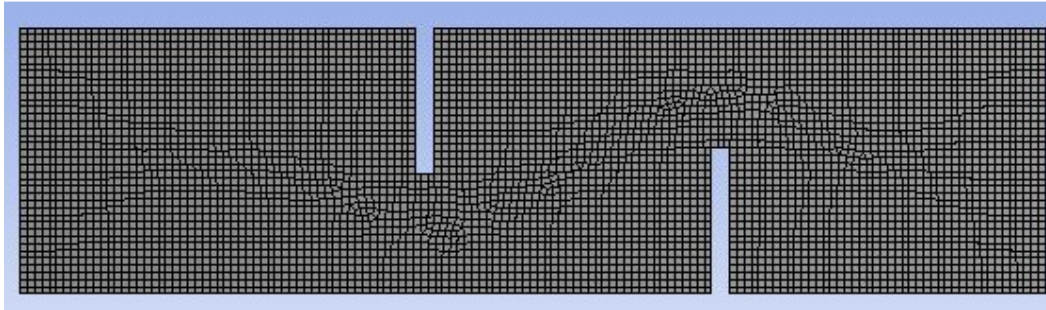


Figure 2: Mesh generated from the entrance along the two baffle plates to the outlet.

4.0 RESULTS AND DISCUSSION

In this study numerical results were obtained from fluent software which are compared with experimental and numerical results reported by Demartine et al. [7] who considered two baffle plates in a flat plate and Numerical results reported by Benzenine et al. [17]. Velocity profiles and separation ability of Reynolds Average Navier Stokes was computed based on three models that include Standard $k-\epsilon$, Realizable $k-\epsilon$ and SST $k-\omega$ around the two baffle plate. The result was computed based on the length of the flat plate, between the entrance, distance between the two plates and the exit region. The existence of velocity at the first phase of the entrance was compared between positions $X=0.159$ and 0.189 respectively. These implies the velocity behaviour at the first baffle plate that shows significant reduction in velocity at upper half of the channel and increase in flow at lower half of the channel.

At the second phase of the channel between $X=0.255$ and $X=0.285$ highest velocity was observed at the lower half of the channel which is paradoxically with upper half of the channel in which negative velocity is obtained as a result of existence of recirculation of flow immediately after the first baffle. In this intermediate region velocity observed was found to be higher than the reference flow velocity.

At the third phase of the channel considered between positions $X=0.315$ and 0.345 the velocity fluctuate as the flow approaches second baffle plate, in the lower half of the channel the velocity was reduced and increased in the upper half of the channel. Eventually, a negative velocity observed just before the second baffle disappear as flow approaches a position of $X=0.345$. Velocity profile in the lower half of the channel approximated almost to null while at the higher half of the channel more air starts over to accelerate again toward the breach above the second baffle.

Lastly, the position $X=0.525$ is the region where maximum velocity was observed which was found to be about 4 times higher than the reference velocity. Highest recirculation behaviour

in the channel was observed immediately after the second baffle. More concern to the velocity behaviour and separation ability of Standard k- ϵ , Realizable k- ϵ and SST k- ω was studied and observation was thoroughly made to which one has the highest separation ability.

4.1 Standard K-epsilon Model Result

Figures 3a- 3d shows velocity distribution behaviours (dimensionless velocity profile) of the flow through the first baffle, intermediate region between first and second baffle and the second baffle plates for the standard K-epsilon simulation.

At position of 0.027m – 0.057m after the first baffle a high velocity of 19.8m/s was obtain at the lower part of the channel. The upper part is characterized by negative velocity value showing the presence of recirculation. For the second baffles towards the exit of the geometry a value of 32.9m/s velocity was observed to be 4.21 times thereference velocity. The high velocity is due to large separation after the second baffle plate.

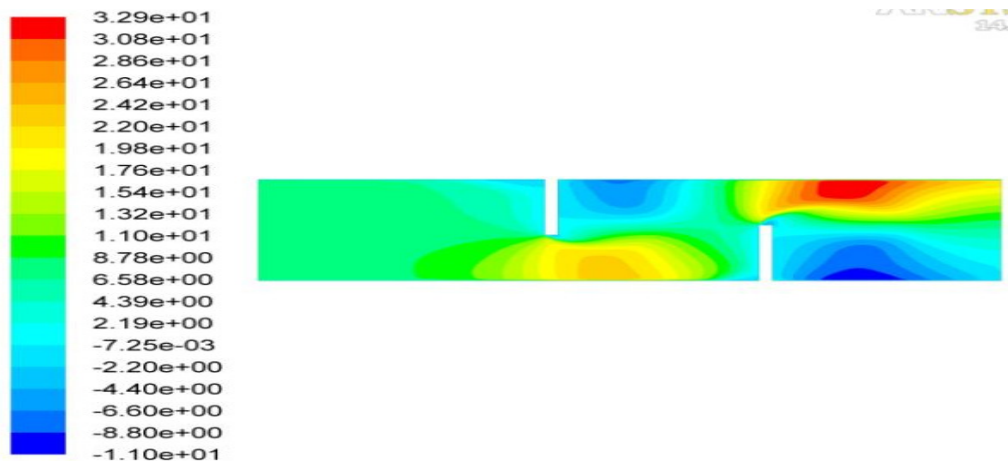


Figure 3(a): Velocity distribution flow from left to right of the duct. (All velocity in m/s)

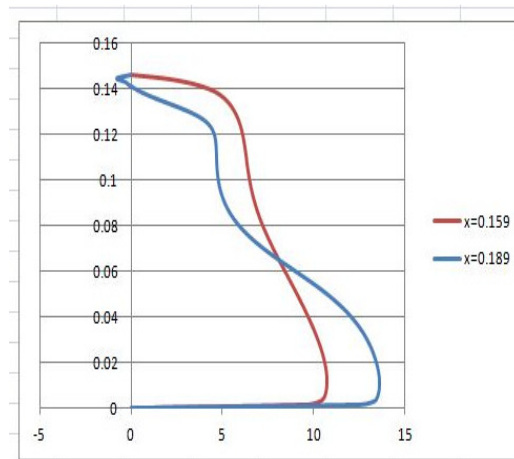


Figure 3(b): Dimensionless velocity profile of the first plate.

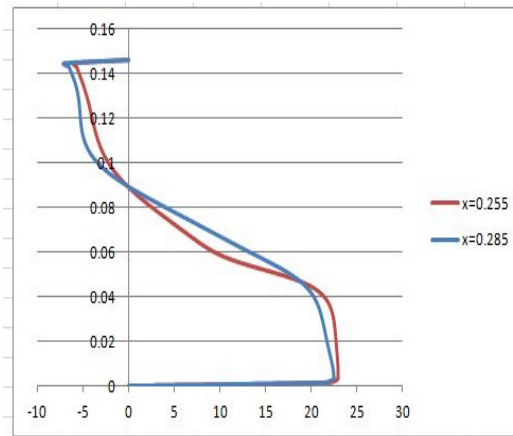


Figure 3(c): Dimensionless velocity profile between the first and the second plate.

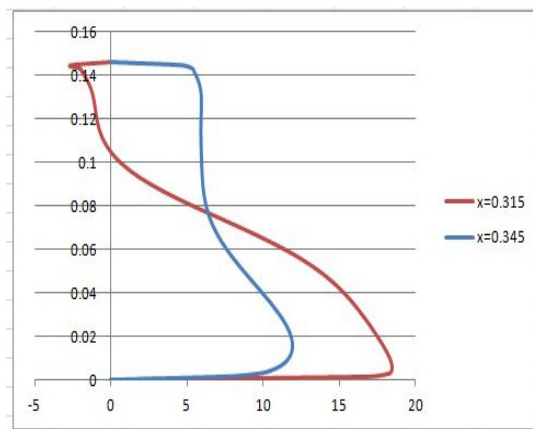


Figure 3(d): Dimensionless velocity profile of the second plate.

4.2 Realizable K-epsilon Simulation

For the realizable K-epsilon a wide range of separation was observed after the first baffle plates with observable negative velocity of 5.3m/s and a high velocity of 25.7m/s at the lower part of the channel. This shows that the velocity is about 329% of the reference velocity (7.8m/s) at position 29mm toward the exit of the channel. After the second baffle a velocity of 31.2m/s was obtained showing an increment of velocity to 400% of the reference velocity. From the differential increment of velocity, it can be shown that the strength of separation after the second baffle is higher than that of the first baffle plate. Figure 4(b)-4c shows the dimensionless velocity profiles of this simulation while Figure 4a shows the magnitude of velocity contour.

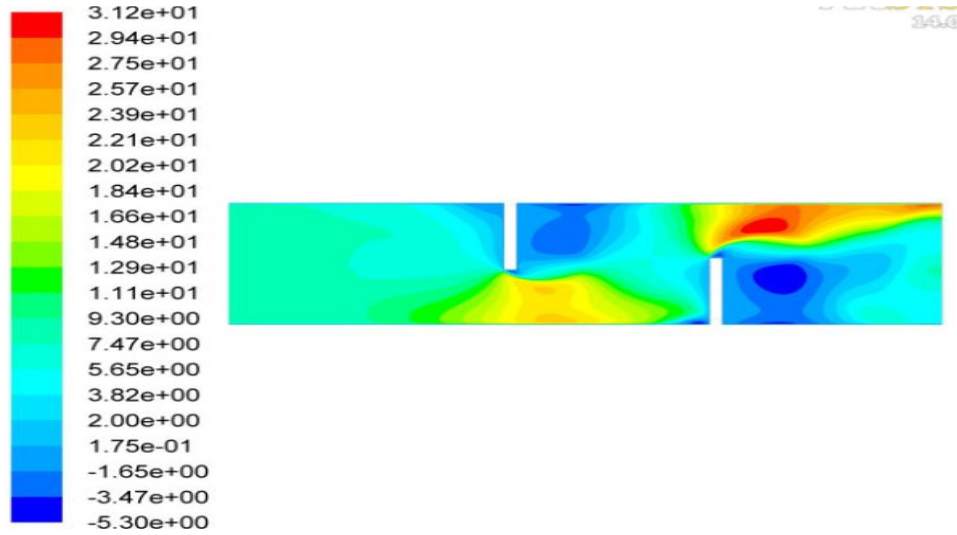


Figure 4(a): Velocity distribution flow from left to right of the duct. (All velocity in m/s)

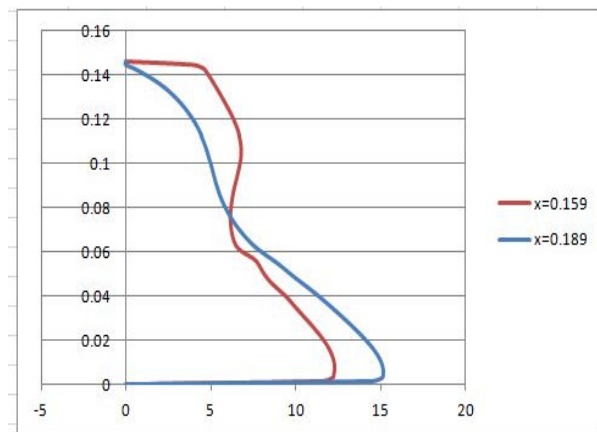


Figure 4(b): Dimensionless velocity profile of the first plate

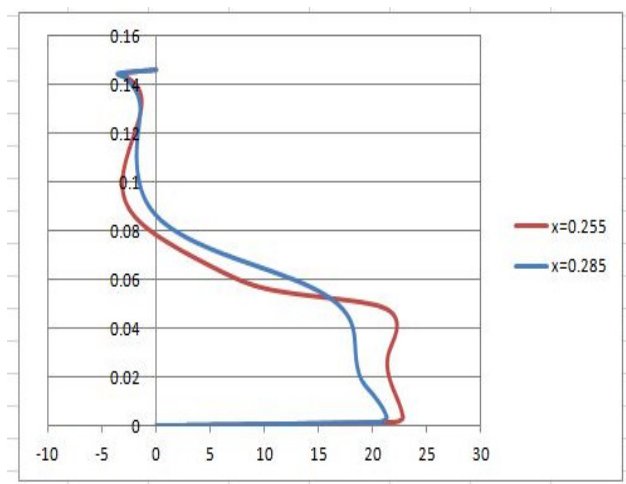


Figure 4(c): Dimensionless velocity profile between the first and the second plate.

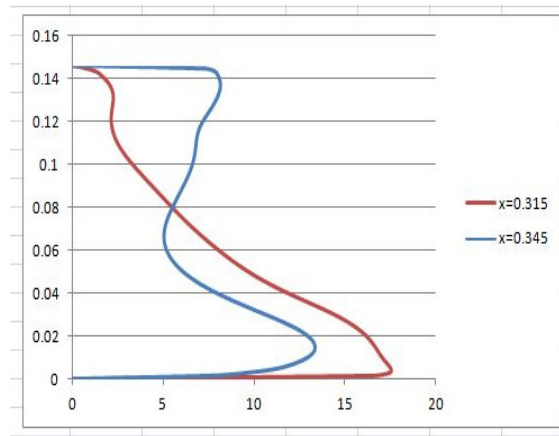


Figure 4(d): Dimensionless velocity profile of the second plate.

4.3 SST K-omega Model

From the velocity contour Figure 5a the velocity reduces as its approaches the first baffle plate thereby increasing the velocity downstream up to a value of 42.7m/s which implies 547% increment of the reference velocity. The magnitude of negative velocity obtained upstream was 45.6m/s indicating high value of separation region after the first plate as the flow moves further after the second plate. The velocity reaches 64.7m/s which also indicate a higher range of separation after the second baffle plate.

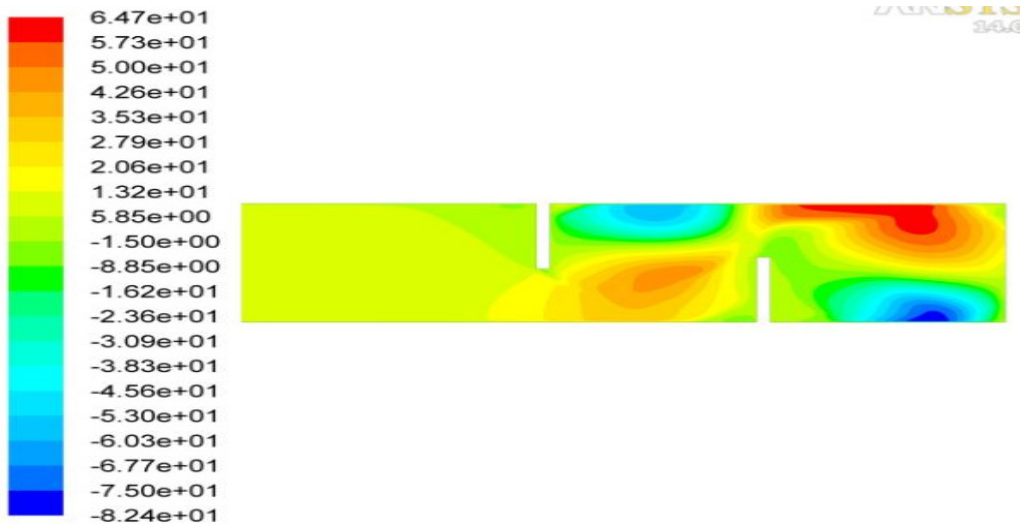


Figure 5(a): Velocity distribution flow from left to right of the duct (all velocity in m/s).

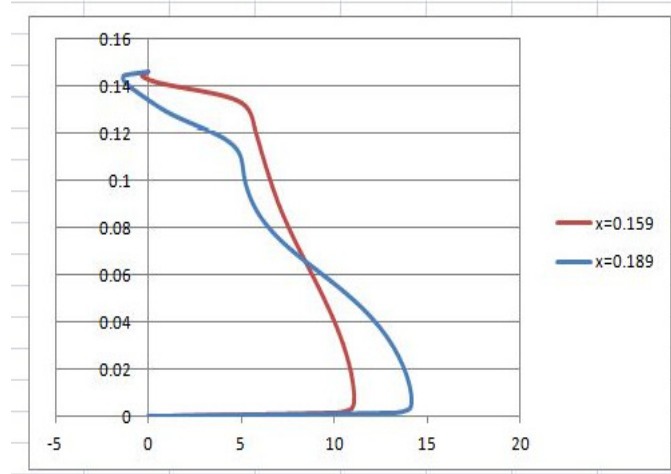


Figure 5(b): Dimensionless velocity profile of the first plate

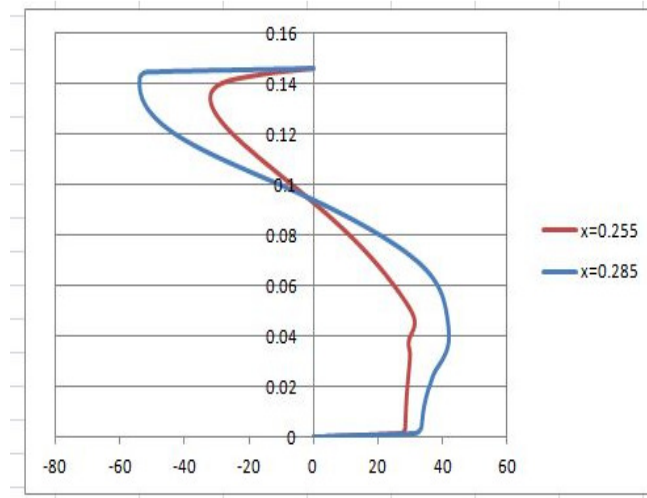


Figure 5(c): Dimensionless velocity profile between the first and the second plate.

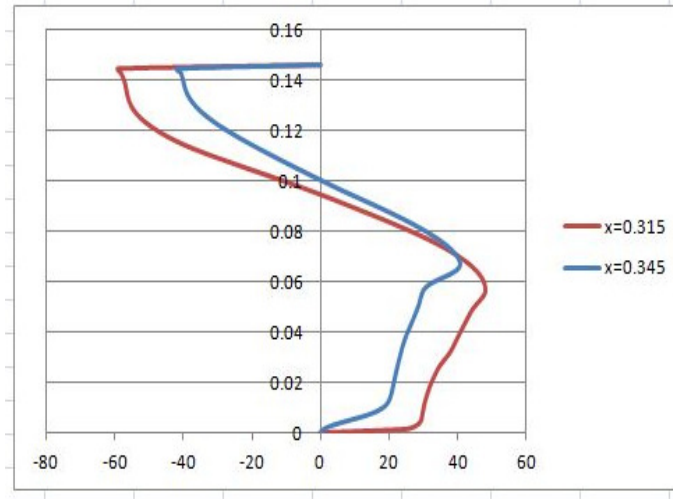


Figure 5(d): Dimensionless velocity profile of the second plate.

4.4 Comparison of Numerical and Validation to Experimental Results

Figure 6 shows experimental results and numerical results of Standard k- ϵ , Realizable k- ϵ and SST k- ω respectively. These comparison was made based on the velocity profile behaviour immediately after the second baffle plate which is near to the channel exit at X=0.525m of the channel position.

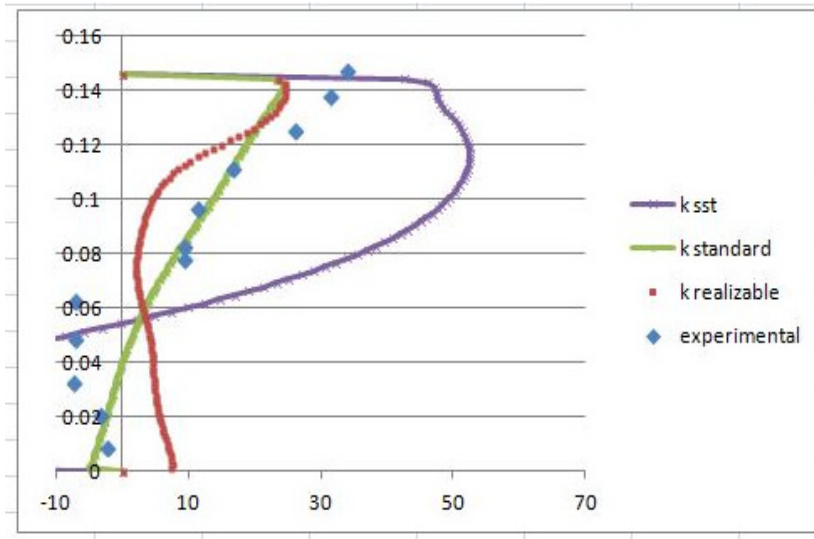


Figure 6: Comparison of velocity profile of experimental, standard k- ϵ , Realizable k- ϵ and SST k- ω at position X=0.525m of the channel.

5.0 CONCLUSION

Turbulent behaviour in a rectangular channel was studied based on Reynolds Average Navier Stoke models of standard $k-\epsilon$, Realizable $k-\epsilon$ and SST $k-\omega$. The geometry of the channel involves two obstacles baffle plates that resembled dynamic flow of heat exchangers that are in shell and tubes.

The flow velocity from the entrance to outlet of the tube has shown remarkable behaviours over certain positions of the channel. Models analysed shows different behaviour of recirculation and separation. The SST $k-\omega$ was observed to show better separation as compared to other two models studied. This is due the ability of the SST $k-\omega$ to change from inner region of the boundary layer to a high Reynolds number of the $k-\omega$ model.

However, the contribution of these models is paramount to turbulence flow through a rectangular channel designed with two baffle plates. All the results obtained have shown realizable agreement between these model and the experimental results obtained. As such, all the three models can be used in general study of turbulence flow in a rectangular channel with different baffles because of the good agreement observed from the models.

REFERENCES

- [1] L..A.M., Endres, S.V. Möller, Experimental study of the propagation of a far-field disturbance in the turbulent flow through square array tube banks, *Journal of the Brazilian Society of Mechanical Sciences and Engineering* 31 (2009) 232-242.
- [2] S. Möller, L. Endres, G. Escobar, Wall pressure field in a tube bank after a baffle plate, *Transactions of SMiRT* 15 (1999) 262-275.
- [3] K. Kelkar, S. Patankar, Numerical prediction of flow and heat transfer in a parallel plate channel with staggered fins, *Journal of heat transfer* 109 (1987) 25-30.
- [4] C. Chin-Hsiang, H. Wen-Hsiung, Numerical prediction for laminar forced convection in parallel-plate channels with transverse fin arrays, *International Journal of Heat and Mass Transfer* 34 (1991) 2739-2749.
- [5] C. Berner, F. Durst, D. McEligot, Flow around baffles, *Journal of heat transfer* 106 (1984) 743-749.
- [6] M. A. Habib, A. M. Mobarak, M. A. Sallak, E. A. Abdel Hadi, R. I. Affify, Experimental investigation of heat transfer and flow over baffles of different heights, *Journal of heat transfer* 116 (1994) 363-368.
- [7] L.C. Demartini, H.A. Vielmo, S. Möller, Numeric and experimental analysis of the turbulent flow through a channel with baffle plates, *Journal of the Brazilian Society of Mechanical Sciences and Engineering* 26 (2004) 153-159.
- [8] Z. Guo, N. Anand, Three-dimensional heat transfer in a channel with a baffle in the entrance region, *Numerical Heat Transfer, Part A Applications* 31 (1997) 21-35.
- [9] S. DeZilwa, L. Khezzar, J. Whitelaw, Flows through plane sudden-expansions, *International Journal for Numerical Methods in Fluids* 32 (2000) 313-329.

- [10] J. Antoniou, G. Bergeles, Development of the reattached flow behind surface-mounted two-dimensional prisms, *Journal of Fluids Engineering* 110 (1988) 127-133.
- [11] M.J. Andrews, B.I. Master, Three-dimensional modeling of a Helixchanger® heat exchanger using CFD, *Heat Transfer Engineering* 26 (2005) 22-31.
- [12] F. Bazdidi-Tehrani, M. Naderi-Abadi, Numerical analysis of laminar heat transfer in entrance region of a horizontal channel with transverse fins, *International Communications in Heat and Mass Transfer* 31 (2004) 211-220.
- [13] R. Saim, H. Benzenine, H.F. Oztop, A.S. Khaled, Turbulent flow and heat transfer enhancement of forced convection over heated baffles in a channel: Effect of pitch of baffles, *International Journal of Numerical Methods for Heat & Fluid Flow* 23 (2013) 613-633.
- [14] M.A. Louhibi, N. Salhi, H. Bouali, K. Amghar, Numerical Analysis of heat transfer in a channel with inclined baffles, *Research Inventy: International Journal of Engineering And Science* 4 (2014) 12-23.
- [15] S. Dahiya, S. Dhingra, M. Kumar, CFD Analysis of Flow Structure of the Dynamic Turbulent Flow Field through a Channel Provided with Baffles, *International Journal of Enhanced Research in Science Technology & Engineering* 3 (2014) 124-132.
- [16] D.C. Wilcox, Comparison of two-equation turbulence models for boundary layers with pressure gradient, *AIAA Journal* 31 (1993) 1414-1421.
- [17] H. Benzenine, R. Saim, S. Abboudi, O. Imine, Numerical simulation of the dynamic turbulent flow field through a channel provided with baffles: comparative study between two models of baffles: transverse plane and trapezoidal, *Revue des Energies Renouvelables* 13 (2010) 639-651.